

Journal of Engineering and Technology DergiPark



Journal of Engineering and Tecnology 6;1 (2025) 1-10

Numerical Model for Thermal Performance Analysis of Panel Radiator

^aSinem Nisa Işıksaçar, ^bMurat Erbaş, ^cAtilla Bıyıkoğlu

- ^aBatman University, Engineering and Architecture Faculty, Mechanical Eng. Dept., BATMAN/TÜRKIYE,
- b,c Gazi University, Mechanical Eng. Dept., Faculty of Engineering, ANKARA/TURKİYE
- ^a sinemnisa.isiksacar@batman.edu.tr, ^b merbas@gazi.edu.tr, ^c abiyik@gazi.edu.tr,

ARTICLE INFO

Article history: Received December 13, 2024 Revised April 4, 2025

Accepted April 24, 2025 Available online June 30, 2025

Key words:

Radiator model

Numerical method

Model validation

Thermal performance test EN 442

* Corresponding author.

E-mail address:

sinemnisa.isiksacar@batman.edu.tr

ABSTRACT

In this study, a numerical model was developed to analyze the thermal behavior of a panel type (PKP) aluminum radiator used for space heating. The developed model was applied to a slice of the radiator and, convection and radiation effects were included in the calculations. Model accuracy tests were performed in the test room located in the Thermal Sciences Laboratory of the Mechanical Engineering Department of the Faculty of Engineering at Gazi University, using the experimental results performed according to the TS EN 442 standard on the market equivalent of the analyzed radiator. The test room was equipped according to the ANSI/ASHRAE-138 standard and made suitable with the EN 442 radiator test. The numerical analysis results showed that; 600-800-1100-1400 W thermal power can be obtained for 30-40-50-60°C temperature differences using the radiator under study and the heat transfer coefficient of the radiator is an average of 6.35 W/m²K.

2017 Batman University. All rights reserved

1. Introduction

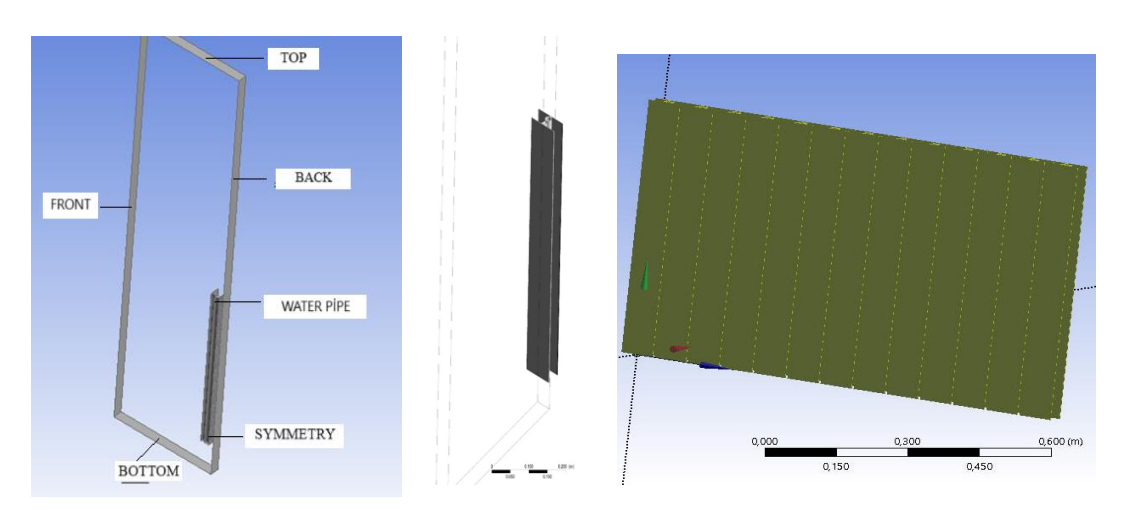
With approximately 45% of the world's total energy consumption, buildings are one of the largest energy consumers [1]. Building heating contributes significantly to this proportion. Therefore, the demand for heating systems with higher efficiency and thermal output is on the increase day by day. One of the most widely used heating devices for the heating of buildings is the panel radiator with convection fins (convector) [2, 3]. Therefore, it is important to increase the thermal output of panel radiators. The thermal performance of panel radiators is affected by the internal fin designs, water channels, and ventilation holes and grilles. In this study, the panel radiator slice is examined and the thermal performance of the radiator is determined. The design of the convectors that are used in the panel radiators has a significant impact on the determination of the total thermal output of the radiator. Therefore, in order to achieve the highest possible thermal output of panel radiators, the geometry and dimensions of the convectors play an important role. For the purpose of getting higher thermal efficiency, it is focused on the internal design of the panel. Although the majority of the heat transfer from panel radiators occurs by natural convection, the contribution of radiation was observed to be around 26% for an inlet/outlet temperature of 75/65 °C [4]. The hot water circulating in the pipes transfers its energy to the ambient air by convection and radiation through the panels and convectors. The temperature difference between the radiator surfaces and the ambient air is the main factor that

causes heat transfer. In order to increase the convective heat transfer, most panel radiators are equipped with convective fins (convectors) [5]. Recent studies have focused on enhancing the thermal efficiency of domestic convectors. Embaye et al. [6] and Calisir et al. [7] examined the impact of pulsating flow regimes on energy consumption in Type 10 and Type 11 convectors. Their findings suggest that constant flow rates fail to optimize heating performance, whereas intermittent flow conditions significantly improve efficiency. Computational Fluid Dynamics (CFD) simulations were employed to analyze localized flow dynamics within the convector systems. Marchesi et al. [8] experimentally compared the thermal behavior of traditional cast iron and modern aluminum convectors under varying hydraulic configurations, flow rates, and mounting positions. Their results demonstrated that aluminum convectors exhibit superior thermal efficiency. Dzierzgowski [9] identified limitations in the EN-442 standard [10], revealing a 22.3% underestimation of thermal output for cast iron convectors under lowflow conditions through tests involving multiple convector types and operational parameters. Calisir et al. [11] analyzed geometric parameters (e.g., panel height, wall thickness, trapezoidal geometry) and concluded that increasing material thickness and panel height enhances heat transfer, albeit at elevated costs. Gritzki et al. [12] questioned the reliability of EN-442 for Type 22 convectors, particularly at reduced flow rates, and explored how inlet-outlet configurations and flow direction adjustments influence heating performance. Beck et al. [13] proposed a novel double-panel convector design incorporating radiative plates, which reduced manufacturing complexity and dust accumulation compared to traditional finned designs but introduced trade-offs in thermal output. Despite these advancements, a systematic investigation linking inlet water temperature, flow rate variations, and localized thermal characteristics in domestic convectors remains absent. This study addresses this gap through experimental analysis of thermal dynamics and the development of a predictive model for average surface temperature.

2. Methodology

2.1 Model Definition

For a radiator with a height of 600 mm, a length of 1000 mm and an inner diameter of 13.3 mm water pipe, the thermal performance of an aluminum panel slice is simulated using ANSYS. The slice width of the radiator is 8 cm and the thickness is 4 cm. A domain size of $460 \times 40 \times 1600$ is used in the analysis. The panel has fins, water pipe and air channels in the rear section, and the geometry and boundary conditions of these components are given in Table-3.



(a) Boundary conditions of model (b) A slice of aluminum radiator model (c) Aluminum radiator model

Figure 1. Numerical model solution domain and boundaries for the radiator slice: (a) Boundary conditions of model (b) A slice of aluminum radiator model (c) Aluminum radiator model

2.2 Governing Equations

In this study, the continuity equation, the momentum equation and the energy conservation equation for the air inside the radiator slice and the radiation equation between the air and the radiator are solved together. The continuity equation is reduced to the following form by the assumption that the Boussinesq equation is incompressible,

$$\vec{\nabla} \cdot \vec{v} = 0 \tag{1}$$

The symbol \vec{v} in Equation (1) represents the velocity of the air.

The momentum equation takes the following form when the effect of buoyancy and viscous forces are taken into account,

$$\vec{\nabla} \cdot (\vec{v} \ \vec{v}) = -\frac{\vec{\nabla}P}{\rho} + \frac{1}{\rho} \vec{\nabla} \cdot \left(\mu \left(\vec{\nabla}\vec{v} + \left(\vec{\nabla}\vec{v}\right)^T\right)\right) - \vec{g}\beta \quad (T - 293.15)$$
 (2)

In this equation, P represents the air pressure, ρ the density of air, μ the viscosity of air and it is assumed to vary with temperature.

The energy equation is reduced to the following form under the influence of advective and conduction terms,

$$\vec{\nabla} \cdot (\vec{v} h) = \frac{1}{\rho} \vec{\nabla} \cdot (k \vec{\nabla} T) \tag{3}$$

The term h in equation 3 is the enthalpy of the air and k is the thermal conductivity of the air.

The discrete ordinate model given in Equation 4 was used to solve the radiative heat transfer between the radiator surface and the surrounding environment simultaneously with the conservation equations.

$$\nabla \cdot (I_{\lambda}(\vec{r}, \vec{s})\vec{s}) + (a_{\lambda} + \sigma_{s})I_{\lambda}(\vec{r}, \vec{s}) = a_{\lambda}I_{b\lambda} + \frac{\sigma_{s}}{4\pi} \int_{0}^{4\pi} I_{\lambda}(\vec{r}, \vec{s}')\Phi(\vec{s} \cdot \vec{s}')d\Omega'$$
(4)

In Eq. 4, λ is the wavelength, a_{λ} is the spectral absorption coefficient and I_{λ} is the radiation intensity.

The turbulence model used was the SST k- ∞ model. Details of the SST k- ∞ model are given in Menter's study [14].

2.3 Material Properties

The characteristics of the aluminium radiator materials used in the market are given in Table-2.

Table 1. Properties of aluminium material used in the analyses

Property	Value	Unit
Density	2719	kg/m³
Specific heat (Cp)	871	J/(kg·K)
Thermal Conductivity	202.4	$W/(m \cdot K)$

The thermophysical properties of air are given in Table-3. The Sutherland model[15] used for dynamic viscosity in the material properties of air is given in Eq. (5).

$$\mu = 1,716 \times 10^{-5} \left(\frac{T}{273,11} \right)^{\frac{3}{2}} \frac{273.11 + 110.56}{T + 110.56} \left[\frac{kg}{m \, s} \right]$$
 (5)

Table 2. Properties of air used in the analyses

Property	Value	Unit
Density	1.11267	kg/m³

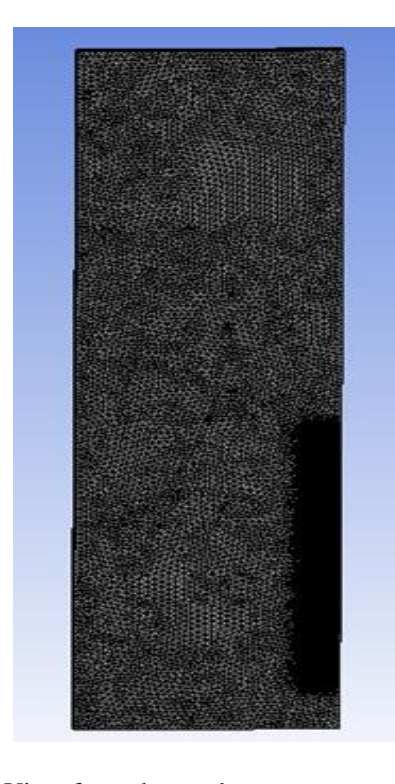
Specific heat (C _p)	Segmented polynomial	J/(kg·K)
Thermal Conductivity	Polynomial	W/(m·K)
Dynamic Viscosity	Sutherland model	kg/(m·s)
Absorption Coefficient	0.01	1/m
Scattering Coefficient	1E-05	1/m
Scattering Phase Function	Isotropic	-
Thermal expansion coefficient	0.00341122	1/K
Refractive Index	1.0003	-

The thermal conductivity polynomial is formed according to the working range and is given in Eq. (6).

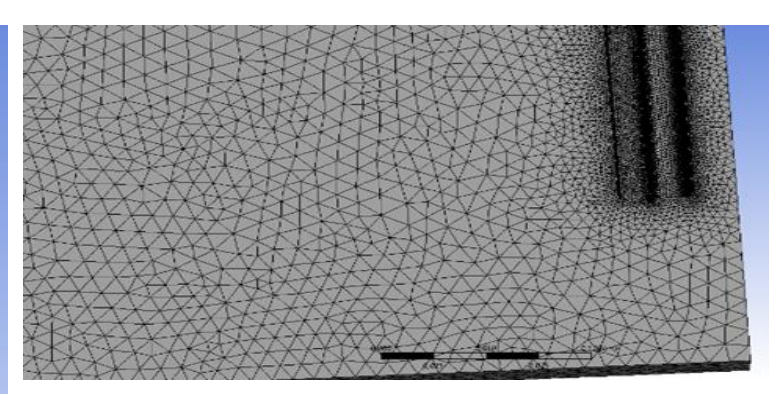
$$k = 1.1144132 \times 10^{-3} + 9,324767 \times 10^{-5}T - 3,63004 \times 10^{-8}T^{2} \left[\frac{W}{mK} \right]$$
 (6)

2.4 Mesh Structure

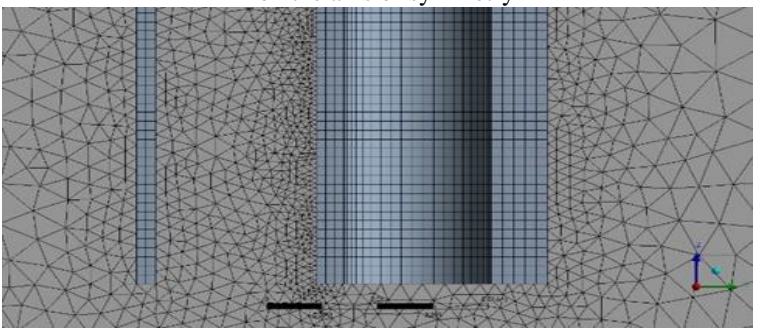
An important parameter that directly affects the accuracy of the model and the reliability of the solution is the mesh structure created for the finite element analysis of the panel slice. In this study, an attempt was made to keep the skewness, number of elements and orthogonal quality values, which indicates the quality of the mesh created to solve the numerical model, at minimum values to ensure convergence of the results and independence from the mesh structure. Accordingly, the number of mesh elements was set to 2.965.115, the maximum value of skewness was set to 0.978 and the minimum value of orthogonal quality was set to 0.1 and the mesh structure was formed as shown in Figure-2.



a) View from the mesh structure on the symmetry axis in the entire solution domain



(b) View from the mesh structure around the panel-water pipe on the axis of symmetry



(c) Symmetry axis view of the mesh structure in and around the panel-water pipe

Figure 2. Solution region used in the numerical model for the radiator slice: (a) View of the mesh structure in the symmetry axis in the entire solution region (b) around the water pipe-panel (c) in and around the panel-water pipe

2.5 Boundary Conditions

The boundary conditions used in the analysis are given in Table-3. The analyses were performed in 4 different ways by applying variable temperature conditions in the water pipe. Constant temperatures were set for the water pipe and different temperature values were applied. Adiabatic conditions were provided on the bottom and back walls and a certain emission coefficient was used for radiation. On the front and top surface, the outlet pressure was defined as 1 atm and radiation conditions were taken into account. For the radiator walls, solid-fluid interface conditions were applied and the radiation emission coefficient was specified.

TO 11 4 D 1	11.1 0		1 1	1	
Table 3. Boundary	z conditions for	numerical	model	solution	region

No	Boundary	BC	Thermal BC		Radiation BC	
		Constant Town	A1	T=50°C		
1 Water pipe	Weter pipe		A2	T=60°C	N/A	
	Constant Temp.	A3	T=70°C	IN/A		
			A4	T=80°C		
2	Ground-back wall	Wall	Adiabatic		ε= 0,98	
3	Front-Top	Pressure Outlet	P = 1 atm		ε=0,98	
4 Radiator Walls		Wall	Solid-liquid		ε=0,95	
4 Radiator Walls	vv an	interface		6-0,93		
5	Symmetry	-	-		-	

3. Introduction of Test Chamber, Test Specimen and Experimental Setup

Capacity determination tests were performed according to TS EN 442-2 standard in test room designed according to ANSI/ASHRAE 138 standard, where air temperature and wall surface temperatures can be controlled, located in Gazi University Mechanical Engineering Department Heat Science Laboratory, shown in Figure-3,4,5.

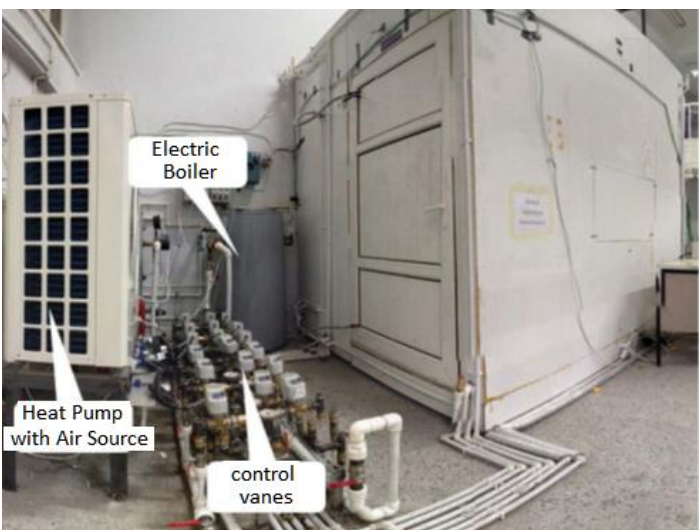


Figure 3. View of the test chamber and mechanical installation equipment

Test samples: MARKET 'Type 21 PKP Aluminium Panel Radiator' The front and top views of the tested radiator are presented below;



Figure 4. Aluminium 600*1000 (13 sections) Radiator - thermocouple locations



Figure 5. View of the radiator test measurement set-up

4. Experimental Method

The panel radiator to be tested is mounted in the middle of the wall in the test room at a height of 50 cm from the floor. The water inlet and outlet temperatures and the water flow rate of the panel radiator are measured. The panel radiator is supplied with hot water at 75°C and the water flow rate is adjusted so that the radiator outlet temperature is 65°C. The indoor temperature of the test room is measured from four different positions (5 cm from the ceiling, 5 cm from the floor, 75 cm and 150 cm) specified in the standard on a vertical rod placed in the centre of the room. The test room is conditioned by cooling from the walls other than the wall where the radiator is located, so that the room temperature is maintained at 20 °C. The average surface temperature of the radiator is calculated using data from three thermocouples placed on the infeed, mid-feed and outfeed surfaces.

Unlike the TS EN 442-2 standard, this test was carried out by feeding water heated by an electric heater in a chamber directly to the radiator by means of a circulating pump. The difference is in the method used to measure the water flow rate, in this test the water flow rate was measured using a calibrated flow meter. The accuracy of the flow meter is ± 0.471 g/s. The method used to determine the thermal output, as specified in the standard, is to measure the water flow through the radiator and to measure the temperatures at the supply and return connections to determine the enthalpy difference.

5. Results

Figure 6 shows the results of the analyses carried out on a section of the radiator at (a) the front, (b) the side and (c) the back. The flow curve and velocity of the ambient air at room conditions are shown. The hottest region in a slice is at the center line. The lower end of the radiator has the lowest temperature. The temperature of the metal increases as it rises. Because the water pipe of the radiator is closer to the back surface, the back surface is hotter than the front surface. The air flow in the radiator is accelerated from bottom to top. As the temperature of the air entering the radiator and the region with the lowest boundary layer thickness is at the bottom, the highest heat transfer coefficient occurs at the bottom.

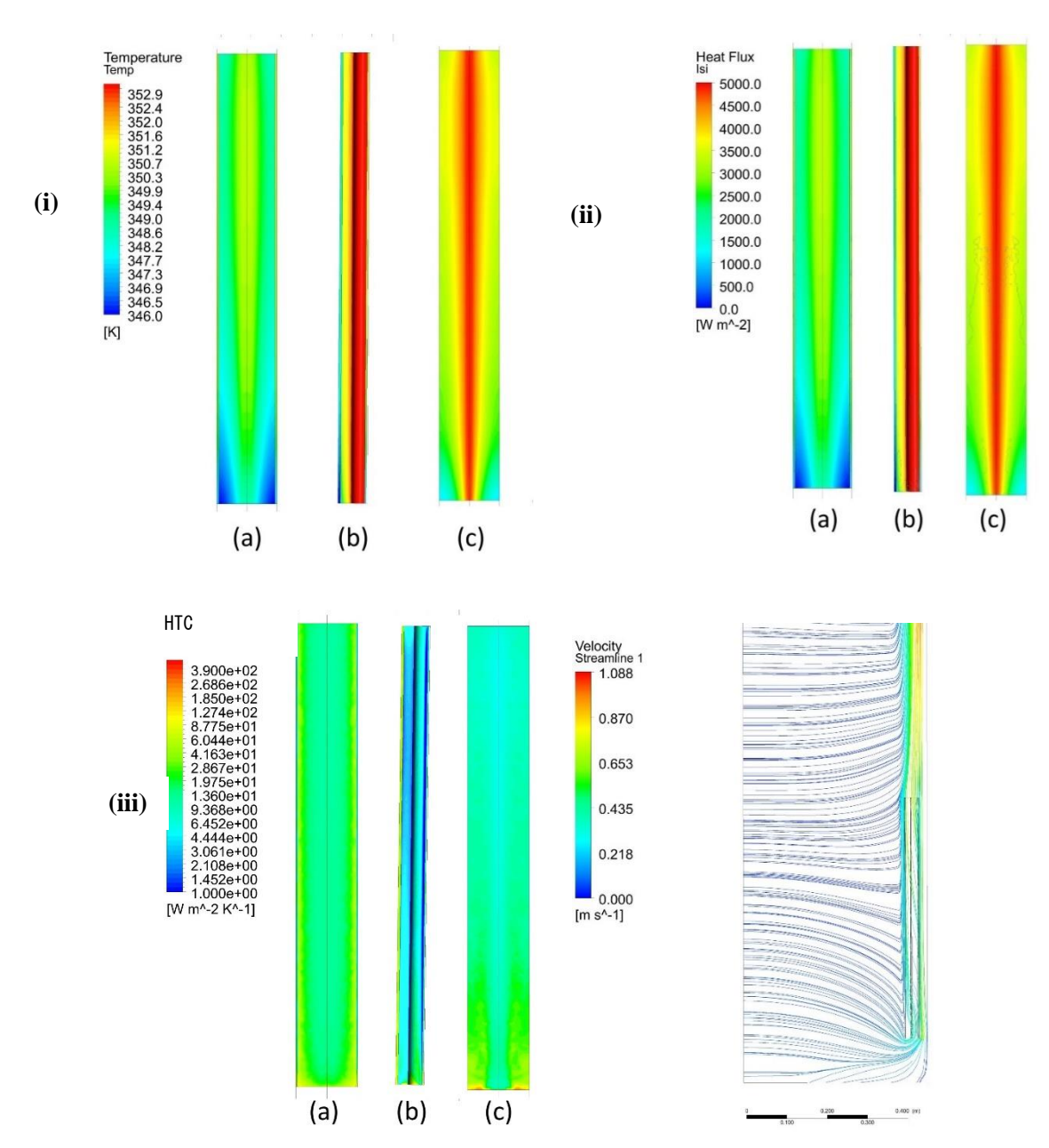


Figure 6. Radiator slice (i) temperature, (ii) heat flux, (iii) heat transfer coefficient (HTC) and air flow (velocity) distributions for $\Delta T = 60 \text{ K}$

The radiator thermal power was calculated by taking the sum of the local heat flux obtained over the water pipe wall as a result of the analysis over the surface area,

$$Q = \int q'' \cdot d\vec{A} \tag{7}$$

and the average heat transfer coefficient was calculated using the following integral,

$$h_{avg} = \frac{1}{A} \int \frac{q'' \cdot d\vec{A}}{T - 293.15}$$
 (8)

The analyzed radiator consists of 13 slices. Therefore, while calculating the radiator thermal power, the numerical result obtained for the slice was multiplied by the number of slices.

The radiator heat transfer coefficient is the same as the radiator slice heat transfer coefficient and is calculated by taking the integral of the local heat flux on the radiator panel surfaces divided by the local temperature difference (difference between local water temperature and ambient temperature) over the total surface as a result of the analysis.

The thermal power and heat transfer coefficients obtained as a result of numerical analysis are given in Table-4.

Table 4. Radiator power and average heat transfer coefficient obtained in the analysis						
Temperature	Water Inlet	Water Outlet	Radiator	Average Heat		
Difference,	Temperature,	Temperature,	Thermal Power,	Transfer Coefficient,		
ΔT [°C]	T _{in} [°C]	T _{out} [°C]	P [W]	<u>HTC</u> [W/m ² K]		
30	55	45	538	5.63		
40	65	55	781	6.15		
50	75	65	1040	6.57		
60	90	70	1335	7.05		

Table 4. Radiator power and average heat transfer coefficient obtained in the analysi

6. Evaluation of The Results

Radiator thermal power values obtained as a result of computational fluid dynamics (CFD) analysis are presented in Figure-6. The market equivalent radiator of the analyzed radiator was tested in accordance with TS EN 442 standard in the test room installed in the Thermal Science Laboratory of Gazi University Faculty of Engineering, Department of Mechanical Engineering. The difference between the average temperature of the water in the radiator and the ambient temperature was 50°C. The radiator thermal power was measured as 1050 W and the heat transfer coefficient was calculated as 7.18 W/m2K. As a result of the numerical analysis, the radiator thermal power was calculated as 1040 W and the heat transfer coefficient was calculated as 6.57 W/m2K. As a result, it was determined that the numerical analysis model gave results compatible with the experiments and its accuracy was proved.

In Figure 7, the radiator thermal powers obtained from the numerical results according to the change of the difference between the average water temperature inside the radiator and the ambient temperature are shown as dots and the correlation curve is shown with a dashed curve. The formulation of the correlation curve obtained in Figure-7 is given by Equation 9.

$$Q = 7,881154 L (\Delta T)^{\frac{5}{4}} [W]$$
(9)

In Eq. (9), ΔT represents the temperature difference [K] and L represents the radiator length [m].

The exponential value of the correlation proposed in the literature for natural convection [16] was found to be 5/4, the same as the value obtained in this study. In the light of these results, it was determined that the model developed for the numerical analysis of the radiator gives results compatible with both the literature and experiments and can be used in different types of radiator thermal power calculations and heat transfer coefficient calculations.

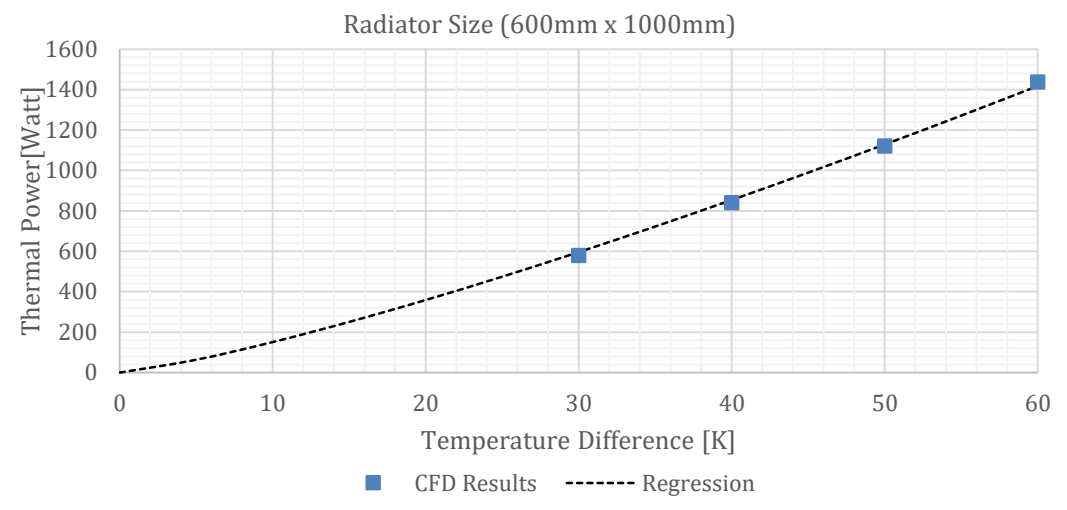


Figure 7. Radiator thermal powers according to temperature difference

Table 5. Radiator power and average heat transfer coefficient obtained in the analysis

Temperature	Experimental	Numerical	Regression	Error Rate (%)
Difference (ΔT)	thermal power	Thermal Power	Estimation (W)	(Experimental vs.
	(W)	(W)		Numerical)
30 K (30°C)	484,0	538	479,6	+10,0
50 K (50°C)	980,4	1040	1048	+5,7
60 K (60°C)	1259,9	1335	1362	+5,7

For $\Delta T = 30^{\circ}$ C, the experimental thermal power (484 W) is approximately 10% lower than the numerical result (538 W) in Table 5. This discrepancy may arise due to weak natural convection at low temperature differences and the model's inability to fully capture boundary layer effects. For $\Delta T = 50^{\circ}$ C and 60°C, the error rate is 5.7%, indicating that the model produces closer predictions to experimental data at higher temperature differences. The regression curve in Equation 9 aligns almost perfectly with the numerical results but shows slight deviations compared to experimental data. This suggests that the regression is based on numerical data and does not fully account for practical limitations in experimental conditions, such as heat losses or measurement precision.

The experimental methodology was meticulously executed in accordance with the TS EN 442-2 standard, thereby ensuring optimal reliability and reproducibility. Tests were conducted in a controlled environment that was compliant with ANSI/ASHRAE-138. In this environment, the temperature of both the walls and the air were regulated with a high degree of precision, with the target temperature set at 20°C. Key parameters, including water flow rate (± 0.471 g/s accuracy) and inlet/outlet temperatures ($\pm 0.1^{\circ}$ C precision), were measured using calibrated instruments, as detailed in the provided test results table. For instance, at a temperature difference of 50°C, the measured thermal power (980.4 W) closely aligns with the numerical prediction (1040 W), with a mere 5.7% deviation, thereby underscoring the consistency of the experimental setup. Furthermore, corrections for barometric pressure effects were applied (e.g., $\Phi = 484.0$ W at $\Delta T = 30^{\circ}$ C), and repeated trials under identical conditions yielded minimal variability, as demonstrated in the tabulated data. The employment of multiple thermocouples for the calculation of surface temperatures, in conjunction with the adherence to the enthalpy-based calculation method stipulated in EN 442, serves to further substantiate the veracity of the results obtained. This meticulous approach aligns with established studies on radiator performance evaluation, thereby reinforcing the credibility of the experimental outcomes for both academic and industrial applications.

References

- [1] Sarbu, I., & Sebarchievici, C. (2015). A study of the performance of low-temperature heating systems. Energy Efficiency, 8(4), 609-627.
- [2] Arslanturk, C., & Ozguc, A. F. (2006). Optimization of a central-heating radiator. Applied Energy, 83(10), 1190-1197.
- [3] Beck, S. M. B., Grinsted, S. C., Blakey, S. G., & Worden, K. (2004). A novel design for panel radiators. Applied Thermal Engineering, 24(11), 1291-1300.
- [4] Calisir, T., Yazar, H. O., & Baskaya, S. (2017). Determination of the effects of different inlet-outlet locations and temperatures on PCCP panel radiator heat transfer and fluid flow characteristics. International Journal of Thermal Sciences, 121, 322-335.
- [5] Myhren, J. A., & Holmberg, S. (2011). Improving the thermal performance of ventilation radiators: The role of internal convection fins. International Journal of Thermal Sciences, 50(1), 115-123.
- [6] Embaye, M., Al-Dadah, R., & Mahmoud, S. (2015). Thermal performance of hydronic convector with flow pulsation—Numerical investigation. Applied Thermal Engineering, 80(1), 109-117.
- [7] Calisir, T., Baskaya, S., Yazar, H. O., & Yucedag, S. (2015). Experimental investigation of panel convector heat output enhancement for efficient thermal use under actual operating conditions. European Physical Journal, 92(2), 02010.
- [8] Marchesi, R., Fabio, R., Claudio, T., Fausto, A., Gino, C., Marco, D., & Giorgio, F. (2019). Experimental analysis of convectors' thermal output for heat accounting. Thermal Science, 23(5), 989-1002.
- [9] Dziergowski, M. (2021). Verification and improving the heat transfer model in convectors in the wide change operating parameters. Energies, 14(17), 6543.
- [10] British Standards Institute. (2014). Convectors Part 1: Technical Specifications and Requirements. BSI Standard EN-442. London, UK.
- [11] Calisir, T., Yazar, H. O., & Baskaya, S. (2017). Determination of the effects of different inlet-outlet locations and temperatures on PCCP panel convector heat transfer and fluid flow characteristics. International Journal of Thermal Sciences, 121, 322-335.
- [12] Gritzki, R., Felsmann, C., Gritzki, A., Livonen, M., & Naumann, J. (2021). Can we still trust in EN 442: New Operating Definitions for Convectors—Part 1: Measurements and Simulations. REHVA, 1(1), 46-53.
- [13] Beck, S., Grinsted, S., Blakey, S., & Worden, K. (2003). A novel design for panel convectors. Applied Thermal Engineering, 24(11), 1291-1300.
- [14] Menter, F. R. (1994). Two-Equation Eddy-Viscosity Turbulence Models for Engineering Applications. AIAA Journal, 32(8), 1598-1605.
- [15] Sutherland, W. (1893). The viscosity of gases and molecular force. Philosophical Magazine, S. 5, 36(5), 507-531.
- [16] Bergman, T. L. (2011). Fundamentals of Heat and Mass Transfer (7th ed.). Department of Mechanical Engineering, Chapter 9: Free Convection